Rheologica Acta
https://doi.org/10.1007/s00397-024-01467-7

ORIGINAL CONTRIBUTION

Effect of urea on the linear and nonlinear rheological properties of human serum albumin hydrogels

Tochukwu Olunna Nnyigide[1] · Osita Sunday Nnyigide[1] · Kyu Hyun[1]

Received: 16 May 2024 / Revised: 24 July 2024 / Accepted: 5 August 2024

Abstract

We report the linear and nonlinear rheological properties of human serum albumin (HSA) hydrogels with and without urea using small (SAOS) and large (LAOS) amplitude oscillatory shear tests. In SAOS tests, pure HSA and HSA-urea hydrogels exhibited a predominantly solid-like behavior ($G' \gg G''$), with viscoelastic properties proportional to HSA concentrations. As urea concentration increased, the viscoelastic properties of the hydrogels decreased and the frequency dependence declined, indicating a sparser cross-linking network. Under LAOS flow, both pure HSA and HSA-urea hydrogels exhibited intra- and inter-cycle strain-stiffening, which became more pronounced with increasing urea concentration. The presence of urea delayed the onset of the nonlinear behavior in HSA-urea hydrogels, in proportion to the urea concentration, decreasing the hydrogel strength. The degree of nonlinearity, quantified by the intrinsic nonlinear parameter Q_0 from Fourier-transform rheology, decreased with increasing urea concentration. Additionally, critical strain amplitudes obtained from LAOS tests indicated that the yield strain of the HSA-urea hydrogels increased with urea concentration. The intracycle behavior was analyzed by sequence of physical processes methods. Molecular dynamics simulations were performed to analyze the hydrogels behavior at the atomic level. Significant changes in the hydrogel network were attributed to the efficient insertion of urea into the HSA hydrogen bond network, which forms the cross-linking network. Thus, the hydrogen bonding between urea and HSA, as well as urea's contribution to HSA denaturation, affects the gelation, linear, and nonlinear viscoelastic properties of the HSA hydrogels.

Keywords Human serum albumin · Urea · Hydrogel · SAOS · LAOS · Molecular dynamics simulation

Introduction

Human serum albumin (HSA), a globular protein, and urea are endogenous molecules synthesized in the liver of all normal functioning humans (Lawn et al. 1981; Arroyo et al. 2014). HSA possesses excellent gelling capabilities and has therefore attracted a lot of interest for the fabrication of hydrogels that are used as mechanical support scaffolds in tissue engineering, and as both internal and external (skin) drug delivery agents (Noteborn et al. 2017; Nnyigide et al. 2023). Supply of HSA was once limited by the availability of human plasma; however, recent advances in recombinant technology have enabled the large scale and economically feasible production of HSA, thus eliminating the need for human plasma collection (Hirose et al. 2010). Urea is a cheap and widely available molecule, produced by the high temperature reaction between carbon dioxide and ammonia (Xiang et al. 2012). It is widely used for medicaments, skincare and beauty products of various types, such as gels, emulsions, and ointments, among others. The moisturizing and denaturation properties of urea have been widely exploited in numerous research and industrial applications (Gasbarro and Solomon 2019; Piquero-Casals et al. 2021). HSA and urea are endogenous, biocompatible, biodegradable, and cheap molecules, and therefore excellent candidates for the fabrication of hydrogels for medical and pharmaceutical applications (Yan and Pochan 2010; Hájovská et al. 2020; Nnyigide et al. 2023).

The demand for hydrogels with novel properties has continued to increase as their applications continue to evolve (Yan and Pochan 2010; Kong et al. 2023; Nnyigide et al. 2023). In addition to their biological characteristics, the mechanical-rheological properties are crucial factors to

✉ Kyu Hyun
kyuhyun@pusan.ac.kr

[1] School of Chemical Engineering, Pusan National University, Busan 46241, Korea

Published online: 16 August 2024

determine the suitability of hydrogels for applications such as drug delivery and tissue engineering (Yang et al. 2015; Ollier et al. 2023). For example, hydrogels for organ-support applications need to possess specific mechanical properties to withstand the stresses exerted by body organs due to gravity and bodily movements according to the desired usage time (Lee et al. 2014). For skin patches, hydrogels need to have mechanical properties similar to those of skin to achieve wearers' comfort and need to remain functional for the intended usage time (Yan and Pochan 2010; Chen et al. 2012). Such diverse requirements of hydrogels' properties evidence the importance of a thorough understanding of the deformation characteristics of hydrogels. Moreover, the evolving demand for hydrogels with novel properties has stimulated active research related to the modification of hydrogels' properties (Yan and Pochan 2010; Nnyigide et al. 2023).

The stress-deformation response of a material is influenced by its microstructure; correspondingly, the applied stress could alter the material's microstructure (Morris 2009; Hyun et al. 2011). Rheological characterizations within the linear viscoelastic (LVE) regime are sensitive to the microstructure of the material and are non-destructive. However, it is now well known that LVE measures are not correlated to the nonlinear viscoelastic properties; hence, their usefulness is limited (Hyun et al. 2002, 2011; Nnyigide et al. 2021; Song et al. 2022b). This is particularly concerning because there are no imposed limits on permissible stresses for hydrogels' actual applications. Therefore, understanding both linear and nonlinear deformation and microstructural dynamics of hydrogels is important for successful applications. To this end, large amplitude oscillatory shear (LAOS) tests have been widely used for understanding nonlinear deformation. Unlike small amplitude oscillatory shear (SAOS) tests, LAOS are not restricted to any regime of strain amplitude or frequency, allowing to investigate materials under arbitrarily set conditions. Additionally, LAOS overcome several inherent problems of other methods, such as edge fracture, wall slip, and shear banding by non-imposition of speed or positional jumps (Hyun et al. 2011; Kim and Hyun 2021; Nnyigide et al. 2021; Song et al. 2022b).

LAOS tests have been recently used to investigate the nonlinear rheological properties of promising hydrogel materials. In addition to the longstanding use of SAOS tests, LAOS tests have now become the protocol of choice for the rheological investigation of many complex fluid systems (Song et al. 2022b; Suman et al. 2023; Nnyigide and Hyun 2023a). For example, SAOS and LAOS tests were used to investigate the linear and nonlinear deformation properties of a heat-induced chitosan/β-glycerol phosphate hydrogel system intended for the construction of injectable biomaterials (Lu et al. 2016). In a recent study, LAOS tests were performed to characterize the nonlinear response of a protein-based hydrogel system made of silk fibroin and hydroxypropyl cellulose for potential drug delivery applications (Cao et al. 2019). In another report, SAOS and LAOS tests were used to characterize heat-set soy protein isolate gels for food industry applications (Xia et al. 2021). Also, a double network hydrogel consisting of κ-carrageenan and polyacrylamide, with wide potential applications, was recently fabricated and characterized under SAOS and LAOS flow, revealing an overall length-scale-dependent linear to nonlinear response. Further analysis, based on Lissajous curves and stress decomposition, identified intracycle strain stiffening along with shear thickening. Thus, the overall structural dynamics of the hydrogel's constituent networks were inferred (Tarashi et al. 2023). Similarly, 4-arm polyethylene glycol (PEG) hydrogels with boronate ester-based cross-linking that mimic the strain-stiffening mechanical response of soft biological tissues were recently reported and characterized via SAOS and LAOS tests. The stiffening behavior, defined by the stiffening index from the LAOS test, decreased with the polymer concentration, whereas the corresponding critical stress values showed a positive correlation. The origins of the observed strain-stiffening behavior were attributed to entropic and enthalpic elasticity (Ollier et al. 2023). Another recent study reported the preparation of hydrogels from glycyrrhizic acid and crosslinked sodium alginate, both as a single network of each and in a mixed double network arrangement, which were compared by SAOS and LAOS tests. Lissajous curves' analysis of the viscoelastic stress–strain data at various strain amplitudes revealed detailed intracycle behaviors associated with the various molecular configurations. Overall, the double network configuration possesses better mechanical properties than the single network counterparts (Li et al. 2023). Hydrogels made from carboxymethyl chitosan (CMCS) and polyvinyl alcohol, with calcium chloride (Ca^{2+}) as the cross-linking agent, formulated for environmental applications in wastewater treatment, were recently studied also using SAOS and LAOS tests. These tests showed that CMCS content determines the overall viscoelastic properties of the hydrogel complex. Additionally, the deformational properties of the hydrogel complexes across length scales were compared via LAOS; the analysis revealed a transition from elastic-dominated deformation to a viscous one (Zhang et al. 2023). Several other studies have demonstrated the importance of the LAOS methodology in unraveling the mechanical and microstructural response of materials over a broad range of shear stress or strain amplitudes. This allows for material classification, establishment of linearity limit, understanding of allowable deformation before structural collapse, and other crucial properties (Nnyigide et al. 2021; Song et al. 2022b; Suman et al. 2023). Despite their evident relevance, studies on the nonlinear rheological behavior of hydrogels based on proteins are scarce. Moreover, LAOS

studies on HSA hydrogels, to the best of our knowledge, have not been reported.

In this work, we present the linear and nonlinear rheological properties and microstructural dynamics of a heat-induced HSA hydrogel containing varying concentrations of urea denaturant. Heat-induced hydrogels of HSA at 3 wt.%, 5 wt.%, and 7 wt.% were prepared with 0–5 M urea. The microstructural information of the hydrogels was obtained from the elastic ($G\prime$) and viscous ($G\prime\prime$) moduli obtained from SAOS tests and atomistic molecular dynamics (MD) simulations. Then, LAOS tests were performed and comparatively analyzed with the results of SAOS and MD simulation by Lissajous curves, Fourier-transform (FT)-rheology, and sequence of physical processes (SPP), to elucidate the microstructural dynamics of the urea-denatured HSA hydrogels.

Experimental

Materials

HSA (lyophilized powder, $M_W \approx 55\text{kDa}$), urea ($M_W = 60.06\text{g/mol}$), and phosphate-buffered saline (PBS) solution were purchased from Sigma-Aldrich (USA) and used as received.

Preparation of the HSA and HSA-urea solutions

PBS was diluted 10 times with distilled water and used as the solvent for the preparation of all samples. HSA powder was then added to a glass vial and dissolved in solutions containing 0–5 M urea to achieve the desired concentrations of HSA (3 wt.%, 5 wt.%, and 7 wt.%). The mixture was stirred using a magnetic stirrer for 2 h before use.

Preparation of hydrogels and tube inversion test

Hydrogels for rheological characterization were prepared by temperature ramping each solution sample using the ARES-G2 rheometer Peltier system, which is discussed further in the next section. Hydrogels for tube inversion tests were prepared by heating the sample-containing vials at 90°C for 2 h using a programmable dry bath and heating block (Gingko, Model no. H2O3-PROIII). Prior to performing the tube inversion test, the resultant hydrogels were cooled to 25°C. Flow characteristics were visually evaluated by inverting or slanting the vials.

Rheological measurements

SAOS and LAOS tests were performed using an ARES-G2 rheometer (TA Instruments, USA). The advanced Peltier system accessory was used to control the temperature, with a 40 mm parallel plate and a 1mm gap. All rheological measurements were carried out under the same conditions. A linear temperature ramp test was used to induce thermal gelation on the protein-urea solutions; samples were heated at a steady rate of 0.5°C/min from 25°C to 90°C. While heating, the LVE properties of the HSA-urea solution were measured at a strain amplitude of 0.01 and an angular frequency of 1 rad/s, with data acquired at a sampling rate of 1 point per 5 s. This was performed to monitor the sol–gel transformation and to determine the gelation temperature (T_{gel}). Subsequently, the HSA-urea hydrogels were linearly cooled to 25°C and subjected to further characterization. A frequency sweep test within the range of 0.1 to 100 rad/s at a strain amplitude of 0.01 was performed on the HSA-urea hydrogels at 25°C. Strain amplitude sweep tests were also carried out on the HSA-urea hydrogels at 25°C with strain amplitude ranging from 0.0001 to 5, at an angular frequency of 1 rad/s. To reduce the effect of experimental artifacts due to accumulated shear history, a five points per decade measurement within the amplitude range was obtained. During each oscillation cycle, 512 data points of shear strain and stress data were acquired using the rheometer software (Trios, TA Instruments) in transient mode. The last of two cycles of oscillation at each strain amplitude was used for data analysis. Sequence of physical processes (SPP) and Lissajous analysis, and FT- rheology were used to examine LAOS data.

Molecular dynamics simulation

The equilibrium structural characteristics and kinetic properties of the HSA-urea solution were investigated by atomistic MD simulation using the GROMACS 2018.7 software on Ubuntu 16.04 LTS. Simulation protocols were as previously reported (Lemkul et al. 2010; Nnyigide and Hyun 2020, 2021, 2023a). The molecular structures of HSA (Sugio et al. 1999) and urea (Knox et al. 2011) were obtained from the Research Collaboratory for Structural Bioinformatics online data bank in PDB (Protein Data Bank) format (Nnyigide et al. 2022). The LVE properties of the HSA-urea hydrogels during cooling from 90°C to 25°C did not vary significantly; hence, molecular conformations should remain the same after gelation (Supporting Information, Fig. S1). All simulations were performed at 90°C, which is above the gelation temperature observed for HSA in urea solution. First, the protein was inserted into a cubic box of $11.346 \times 11.346 \times 11.346$ nm, after which the desired concentration of urea was added. Thereafter, the box is solved using the simple point charge model of water, and in accordance with concentrations. An example simulation box can be found in Fig. S2 (Supporting Information). HSA was simulated with 0, 1, 3, and 5 M of urea (Supporting

Information, Table S1). The GROMOS 53A6 force field, which has been well optimized for biomolecules, was used for the calculation of inter-particle interaction (Oostenbrink et al. 2004). To stabilize the system and minimize artifacts in the production run, an energy minimization step using the steepest descent algorithm was applied first. Thereafter, NVT (constant number of particles, volume, and temperature) and NPT (constant number of particles, pressure, and temperature) equilibration steps, lasting 2 ns each, were performed to further relax the system. The production MD simulation run was performed for a duration of 150 ns. All simulations were carried out following the same procedures.

Results and discussion

Heat-induced gelation of HSA-urea solutions

The transformation of HSA-urea solutions into hydrogel was characterized by heating from 25°C to 90°C at a constant rate of 0.5°C/min, which was followed by cooling to 25°C. During temperature ramping, the viscoelastic properties measured under LVE conditions (strain amplitude = 0.01, angular frequency = 1 rad/s) provided evidence of gelation, and the gelation temperature (T_{gel}) can be determined. The changes in viscoelastic properties ($G\prime$ and $G\prime\prime$) are illustrated in Fig. 1a.

The solution and gel states correspond to completely different microstructural conformations of the protein molecules (Le Bon et al. 1999; Nnyigide et al. 2023). The initial $G\prime$ values were low ($\sim 10^{-3}$Pa) and randomly fluctuated with temperature before 68°C. This region corresponds to the solution (sol) state. Native proteins have four-tiered structural complexity with a three-dimensional (3D) fold that correlates to their function (Le Bon et al. 1999; Ghosh et al. 2009). Specifically, native HSA is globular and may be approximated to a sphere. In aqueous solutions, proteins are easily dissolved because of the hydrophilic and charged residues on their surfaces; urea solvation is enabled by its hydrogen bonding interaction with water molecules (Nnyigide and Hyun 2020; Piquero-Casals et al. 2021; Nnyigide et al. 2021). Although easily dissolved, long-range repulsive interactions between dissolved native proteins prevent aggregation, resulting in no significant changes in $G\prime$, as observed at temperatures below 68°C (i.e., sol state) in Fig. 1a. However, perturbations such as increased thermal energy, pH changes, or the presence of other molecules, may disrupt or change the stability range of the protein interactions, leading to unfolding. When proteins unfold, their typically buried hydrophobic residues become exposed. In such instances, molecules may aggregate through interactions like localized electrostatic attraction, physical cross-linking, or hydrogen bonding. If such aggregation reaches dimensions that are within the scale of a bulk system, an increase in $G\prime$ is observed (Le Bon et al. 1999; Nicolai 2019), as seen in Fig. 1a. The T_{gel} corresponds to the onset temperature of sol–gel transition, i.e., the temperature where aggregation levels are sufficient to change the overall characteristics from that of solution into gel behavior. T_{gel} values correspond to the temperature where $G\prime$ starts to evolve after equaling or exceeding $G\prime\prime$. In general, protein gelation consists of two processes, unfolding and aggregation. T_{gel} is an important characteristic which determines their potential for different applications (Pieklarz et al. 2022; Nnyigide and Hyun 2023b). Without additives, HSA gelation kinetics display low sensitivity to concentration, while its viscoelastic properties tend to increase linearly with concentration (Nnyigide et al. 2023). The gelation curves of HSA solutions and the effect of increasing urea concentrations are shown in Fig. S3. For pure HSA, T_{gel} slightly decreased as concentration increased (T_{gel}= 77°C, 71°C, and 68°C for 3 wt.%, 5 wt.% and 7 wt.% HSA); differences in cross-linking density were the only change on viscoelastic properties. Urea is a well-known protein denaturant. It has been suggested that its denaturing effect stems from its interaction with the hydrophobic residues of the protein and the disruption of structural hydrogen bonding due to its stronger hydrogen bonding affinity compared to that of several peptide residues (Nnyigide et al. 2018; Piquero-Casals et al. 2021). As shown in Fig. 1b, the gelation temperatures decreases steadily as the

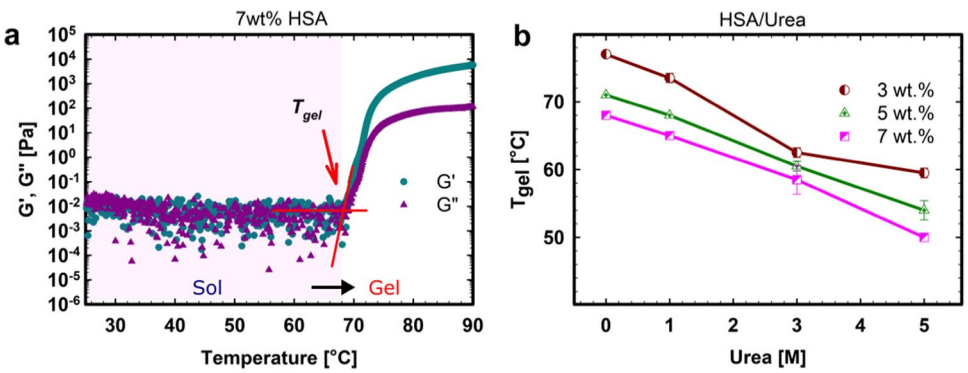

Fig. 1 (**a**) The storage and loss modulus (G' and G") as a function of temperature for the 7 wt.% HSA solution. (**b**) T_{gel} of 3 wt.%, 5 wt.% and 7 wt.% HSA with 0–5 M urea

urea concentration increased. The lowest T_{gel} values, were observed with 5 M urea (59°C, 53°C, and 50°C for 3 wt.%, 5 wt.%, and 7 wt.% HSA).

Hydrogels prepared via constant heating using a dry bath at 90°C are presented in Fig. 2. All hydrogels remained stable when the tube was inverted, with no observed flow except for 3 wt.% HSA with urea concentrations greater than 1 M. Specifically, 3 wt.% HSA formed soft gels with 3 and 5 M urea, displaying a slow flow when the vial was tilted. To quantify the linear viscoelastic properties, SAOS tests were conducted.

Linear viscoelasticity of HSA-urea hydrogels

The LVE properties of pure HSA and HSA-urea hydrogels were investigated as a function of angular frequency. The strain amplitude of 0.01 used for the frequency sweep measurements was confirmed to lie within the LVE limit by a strain amplitude sweep of pure 3–7 wt.% HSA hydrogels, as shown in Fig. S4a. Figure 3a shows the LVE properties of pure HSA hydrogels, which behave as viscoelastic solids ($G\prime \gg G''$) within the entire frequency range, indicating that the HSA chains are stably and irreversibly crosslinked. The values of $G\prime$ and G'' increase with increasing HSA concentration, suggesting a rise in cross-linking density. Usually, hydrogels made of biological materials such as HSA have 3D structures of varied dimensions, resulting in a spectrum of relaxation times (Turco et al. 2011; Khodadadi and Sokolov 2015). LVE measurements together with power-law rheology have been utilized to study the microstructure of protein hydrogels

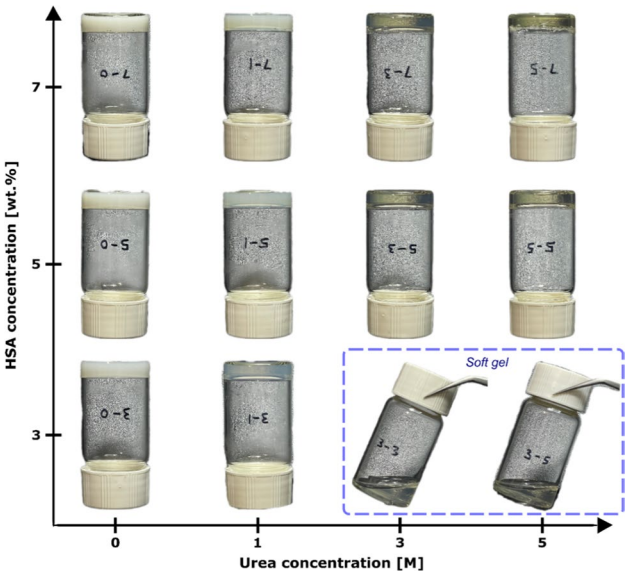

Fig. 2 Images of HSA hydrogels containing 0–5 M urea after heating at 90°C for 2 h. Tube inversion tests were carried out at 25°C

(Aufderhorst-Roberts et al. 2023). Insets of Fig. 3a show the variation in frequency dependence for normalized $G\prime$ and G''. As protein concentration changes, $G\prime$ shows scaling variations with frequency, while G'' does not. Notably, a large increase in $G\prime$ with frequency is observed as the protein concentration increases, while G'' shows no variation. The scaling behavior of $G\prime$ suggests an increasingly dense crosslinked network of smaller structures as HSA concentration increases. Contrarily, the lack of scaling changes in G'' suggests that the short structures were predominantly elastic within the length scales probed under SAOS flow.

The effect of urea on the LVE properties of the HSA-urea hydrogels is shown in Fig. 3b. The insets correspond to $G\prime$ and G'' normalized by their maximum values, thus compare the scaling behavior with respect to frequency. For the 7 wt.% HSA hydrogels containing 0–5 M urea, a predominantly solid-like behavior was observed ($G\prime \gg G''$). However, as urea increases, the magnitude of the moduli ($G\prime$ and G'') decreased, suggesting a reduction in the hydrogel cross-linking density. As observed from the inset plots, the frequency dependence of $G\prime$ and G'' similarly decreased, indicating a more sparse/porous 3D structure of the overall gel network. The frequency sweep behavior of all hydrogels is shown in Fig. S4a. It is worth noting that all hydrogels show a dominant solid-like behavior under SAOS measurements in the range of 0.1–100 rad/s, except for 3 wt.% HSA with 5 M urea which shows a crossover ($G\prime\prime > G\prime$) at high frequency.

Winter and Chambon (1986) showed that the frequency dependence of the moduli, $G\prime(\omega)$ and $G''(\omega)$, exhibits distinct scaling properties at the gel point, i.e., at $G\prime = G''$. The frequency dependence prior to gelation, at the polymer solution state, is such that $G\prime \sim \omega^2$;$G'' \sim \omega$. The solid state is characterized by a frequency dependence where $G\prime \approx constant$;$G'' \sim \omega$. However, several hydrogels show weak dependence of $G\prime$ on frequency, i.e., $G\prime \sim \omega^n$;$1 > n \gtrsim 0$ (Aufderhorst-Roberts et al. 2020; Wang et al. 2021; Tarashi et al. 2023; Aufderhorst-Roberts et al. 2023). The moduli of 7 wt.% pure HSA and the corresponding HSA-urea hydrogels were fitted to the power-law of the frequency ($G\prime \sim \omega^{\alpha}$ and $G'' \sim \omega^{\beta}$). The power-law exponents α and β, which are sensitive to the hydrogel microstructures, are compared in Fig. 3c. The power-law viscoelasticity was confirmed by scaling of the complex viscosity with frequency (Fig. S4b). For pure HSA and HSA-urea hydrogels, $G\prime$ shows a much weaker dependence on frequency than G'', as expected. For the pure HSA hydrogels, the value of the exponent α increased with HSA concentration and ranged from 0.058 to 0.085, while β was constant (~0.145). However, both α and β values decreased with urea concentration in the HSA-urea hydrogels. The magnitude decrease of the moduli and the significant changes in frequency dependence observed

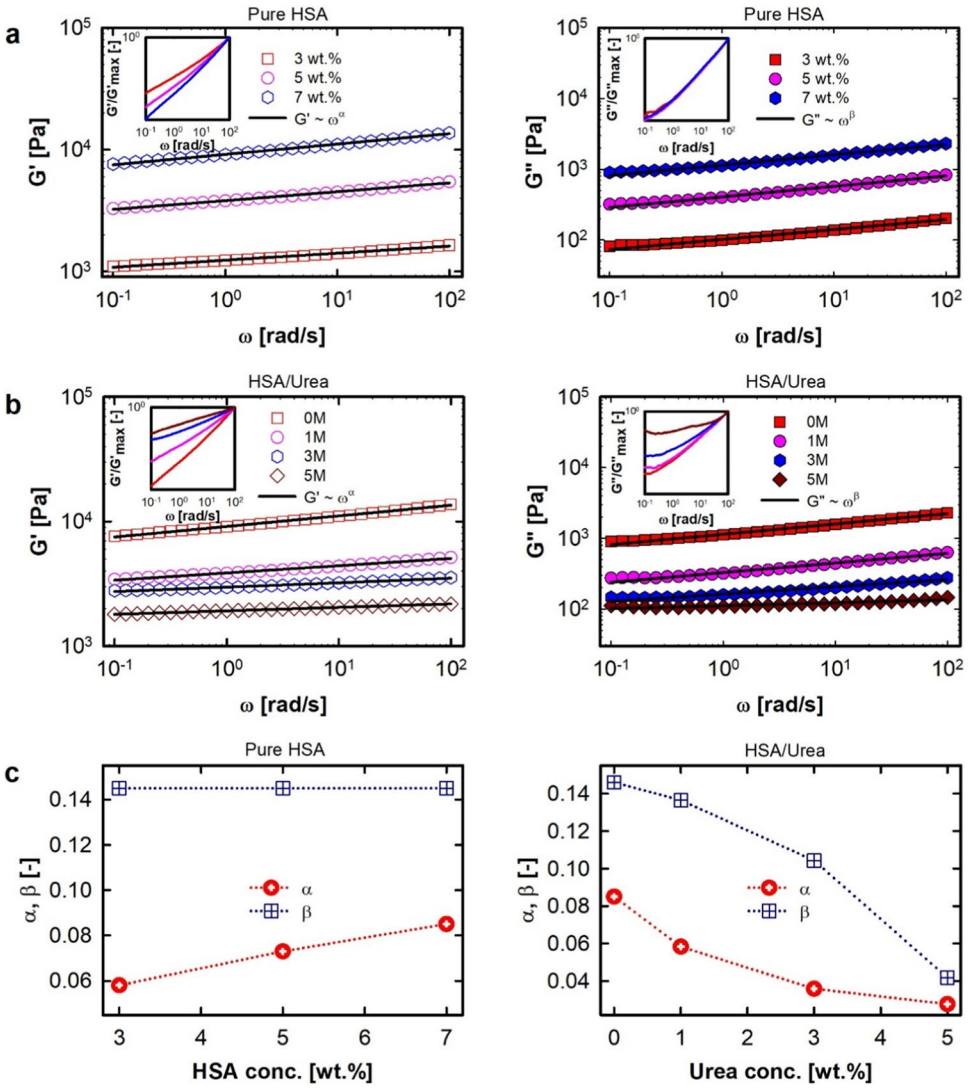

Fig. 3 Viscoelastic moduli (G' and G'') obtained from frequency sweep tests (symbols) and power-law fits (solid lines) of (**a**) pure 3 wt.%–7 wt.% HSA and (**b**) 7 wt.% HSA containing 0–5 M urea; insets show the corresponding normalized values. (**c**) Power-law parameters (α and β) corresponding to pure HSA (Fig. 3a) and HSA-urea hydrogels (Fig. 3b). Frequency sweep tests were carried out at 25°C

through the power-law exponents, suggest significant changes in the hydrogel microstructure as urea concentration increases.

Molecular dynamics simulation of HSA-urea hydrogels

MD simulation was carried out to investigate the equilibrium microstructure of the HSA-urea hydrogels. The transformation of the HSA solution into a hydrogel is a multistep process that includes denaturation and aggregation, generally associated with the loss of high-order protein molecular structures (Le Bon et al. 1999; Ghosh et al. 2009; Nicolai 2019). HSA, like most proteins, undergoes heat-induced denaturation. The denaturation process is also influenced by the presence of urea, a known denaturing agent (Nnyigide et al. 2018; Nicolai 2019).

To better comprehend the gelation process, protein unfolding, and molecular conformational properties calculated from MD simulation trajectories are commonly used (Baler et al. 2014). Parameters derived from the MD simulation of HSA with varying concentrations of urea are shown in Figs. 4a–c. The secondary structure count of HSA in solutions with urea is shown from time 0 to 150 ns of the MD run (Fig. 4a). Higher urea concentrations result in higher HSA unfolding, i.e., HSA's secondary structure decreased more rapidly over time with higher urea concentrations. The inset in Fig. 4a shows the average solvent accessible surface area (SASA) of HSA molecules at different urea concentrations. SASA values are well correlated with protein structures (Durham et al. 2009; Nnyigide et al. 2018); the SASA increase with urea concentration suggests a higher unfolding rate, which agrees with the secondary structure count.

The radial distribution functions (RDF), g(r), of urea from the HSA surface are shown in Fig. 4b and the RDF of

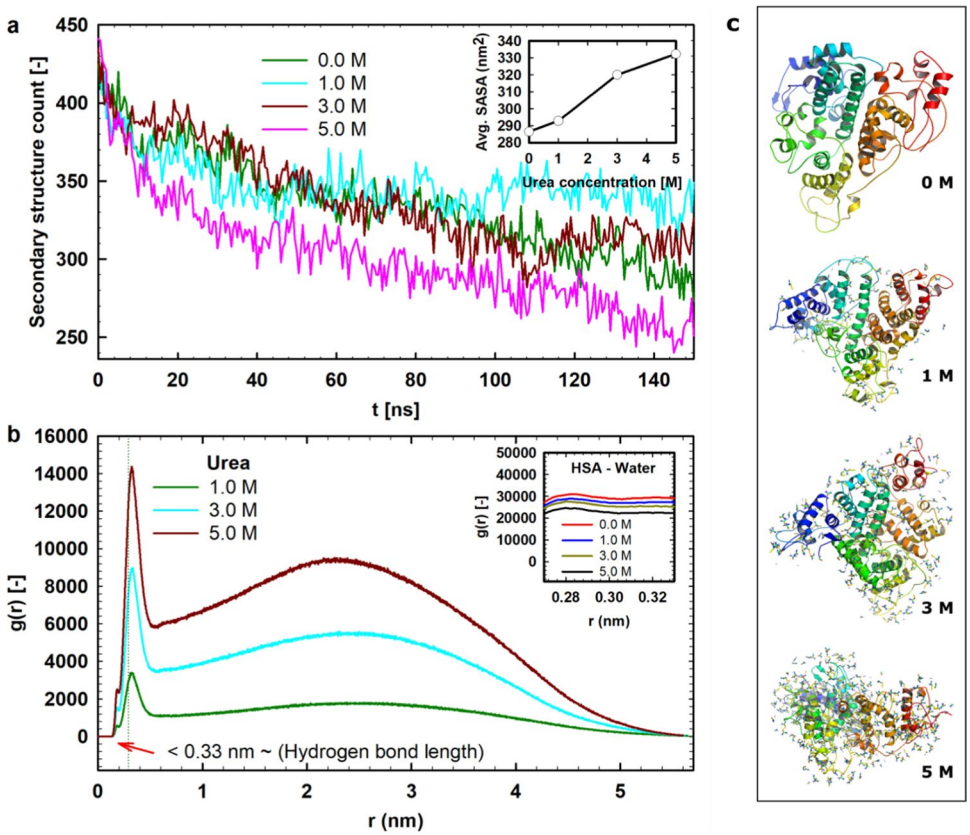

Fig. 4 (**a**) Secondary structure count of HSA in presence of 0–5 M urea; inset shows the solvent accessible surface area (SASA). (**b**) Radial distribution of urea from the HSA surface, inset shows the radial distribution of water from HSA surface. (**c**) Snapshots at 150 ns showing regions within 5 nm from the protein surface

water from HSA surface is shown in the inset. For brevity, only the length scale that corresponds to HSA-bound water, i.e., hydration water, is shown in the inset plot. The RDFs suggest that urea increasingly displaced water from regions close to the HSA surface. The amount of bound urea, and displaced water, is proportional to urea concentration. The snapshots at 150 ns (Fig. 4c) show that urea molecules surround and interpenetrate the HSA structure. Urea molecules can form up to six hydrogen bonds, thus can interact with the HSA surface and other urea molecules. They are well known to interact with both hydrophilic and hydrophobic surfaces hence their ability to permeate HSA (Nnyigide et al. 2018; Piquero-Casals et al. 2021). The disruptive features of the HSA-urea interaction, such as the disturbance of the HSA's structure-stabilizing hydrogen bond network, and screening of charges, lead to rapid HSA structural unfolding. Gelation, which follows unfolding, exhibits analogies to chemical reactions where reactants (unfolded chains) undergo a cross-linking reaction to form a product (gel network). The evolution and final values of the moduli ($G\prime$ and $G\prime\prime$) that correlate with the resultant gel fractals depend on two different rate-limiting steps. When the protein chain cross-linking rate is faster than the diffusion of the unfolded chains, such gelation is said to be diffusion-rate limited. The opposite scenario is referred to as reaction rate limited. For HSA, and most proteins, gelation is diffusion-rate limited. The calculated HSA diffusion coefficient from the MD trajectory decreased linearly ($R^2 = 0.95$) with urea concentration (Fig. S5a). Also, MD simulation shows that normalized $G\prime$ increased with normalized diffusivity, suggesting that more cross-linking and stronger hydrogels are in consonance with the diffusion rate of the HSA chains (Fig. S5b). The rapid unfolding observed in the SASA and RDF values agrees with the decrease in gelation temperatures. Moreover, the reduction in cross-linking density (decreasing moduli) may be explained by the falling diffusivity of the protein chains as urea concentration increased. Such reduced cross-linking density is expected because protein cross-linking is likely driven by hydrophobic and charged interactions, which are reduced by urea binding. The decrease in the density of HSA physical crosslinks, caused by slow diffusion after urea binding, may be comparable to the reduced ability for close packing of other polymeric systems introduced with branching (French et al. 2021; Fan et al. 2022).

Nonlinear viscoelasticity of HSA-urea hydrogels

While simple and effective, LVE measurements do not offer a comprehensive insight of the material's processing flow characteristics and microstructure. This limitation arises due to the inherent constraint of LVE to small deformations, a requirement that is not always met in material applications

(Hyun et al. 2002, 2011; Song et al. 2022b). To overcome this, LAOS tests were performed for pure HSA and HSA-urea hydrogels. In LAOS testing, the oscillatory shear strain amplitude is swept, typically at logarithmic intervals, from small to large values, while observing the properties of the material. A typical LAOS result is shown in Fig. 5a for the 7 wt.% HSA hydrogel. The deformational response ($G\prime$ and $G\prime\prime$) to the applied strain amplitude can be grouped into three regimes, depending on the nature of the resulting stress: (I) SAOS, (II) MAOS, and (III) LAOS. When the strain amplitude is small and at a fixed frequency, the corresponding stress signal is sinusoidal with the same frequency as the strain, and the corresponding regime is called SAOS. In this regime, the hydrogel material functions do not change significantly and are thus linear. The normalized elastic (green) and viscous (red) Lissajous curves (Fig. 5a insets) are ellipsoidal in the SAOS regime. The MAOS regime is found in between the SAOS and LAOS. Therein, the stress response shows subtle deviations from SAOS as the output response gradually departs from pure sinusoid due to growth of odd higher-order harmonics. Properties in the MAOS regime, such as those represented by the Lissajous curves, are asymptotic deviations from their SAOS counterparts. This regime has been characterized using only two harmonics of the stress signal: the first (I_1) and third (I_3) harmonic intensities. In the LAOS regime, the hydrogel material functions change with strain amplitude and are thus nonlinear. The LAOS regime is characterized by the presence of many higher-order harmonics that result in a stress signal that can significantly depart from the SAOS and MAOS regimes. Ideally, only odd harmonics are present in the stress response. However, even harmonics may be present due to experimental deficiencies. The ratio of the third to the first harmonic intensities ($I_{3/1} = I_3/I_1$) as a function of strain amplitude is shown in Fig. 5b for the 7 wt.% HSA. The magnitude and scaling changes of $I_{3/1}$ show the progression

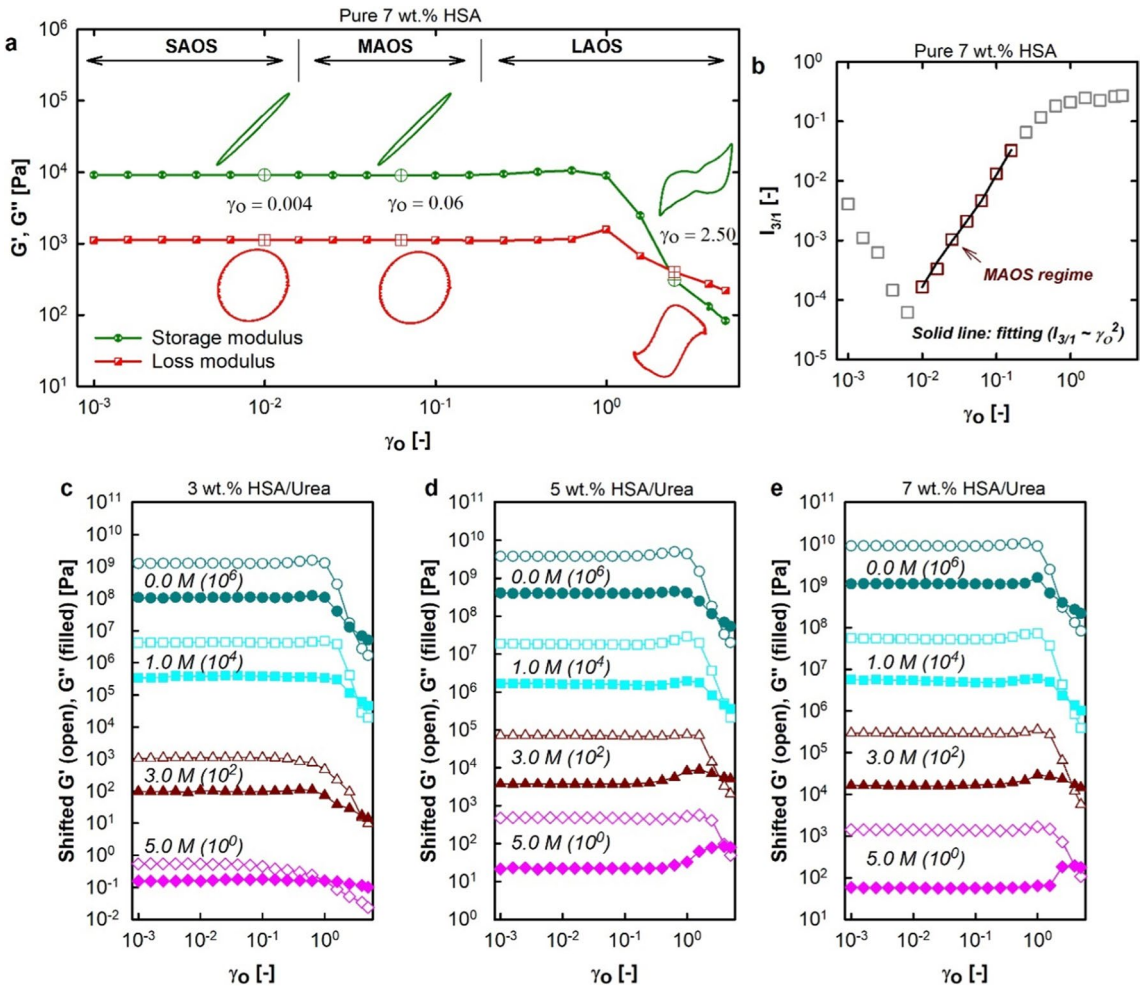

Fig. 5 (**a**) LAOS test results for the 7 wt.% HSA hydrogel, elastic and viscous Lissajous curves are shown as insets. (**b**) $I_{3/1}$ as a function of strain amplitude for the 7 wt.% HSA hydrogel. Strain amplitude sweep (0.1–500%) for the (**c**) 3 wt.%, (**d**) 5 wt.%, and (**e**) 7 wt.% HSA with 0–5 M urea. Strain sweep tests were carried out at 25°C. The results are arbitrarily shifted for easy comparison

of the nonlinearity of the stress response and indicate the SAOS, MAOS, and LAOS regimes. However, the MAOS regime is characterized by a quadratic scaling of $I_{3/1}$ with respect to the strain amplitude. The strain amplitude sweep tests for the of 3 wt.%, 5 wt.%, and 7 wt.% HSA hydrogels containing 0–5 M urea are shown in Figs. 5c, 5d, and 5e. The strain sweep results were shifted by arbitrary shift factors for brevity, and the shift factors are indicated for each curve.

The normalized elastic Lissajous patterns (stress–strain plots) of the HSA hydrogels with different urea concentrations are shown at different strain amplitudes in Figs. S6–S8. Within the LVE regime, all Lissajous stress–strain hysteresis plots traced exact ellipses. However, at larger strain amplitudes, the Lissajous curves deviated from their elliptical shapes due to the onset of nonlinearity. The deviation from a perfect ellipse is due to the presence of higher-order harmonics of the base frequency. Overall, the shape changes indicate that the HSA-urea hydrogels exhibit nonlinear intracycle strain-hardening beyond the LVE regime. However, even though Lissajous patterns can identify the onset of nonlinearities, they do not provide a quantitative measurement. To achieve a quantitative understanding of the nonlinear rheological behavior of HSA-urea hydrogels, three different approaches were employed: (i) zero-strain intrinsic nonlinear parameter (Q_o) from FT-rheology, (ii) analyses of yielding behavior from critical strain amplitude, and (iii) analysis of the SPP transient moduli. Through these methods, the nonlinearity of the HSA-urea hydrogels can be elucidated beyond what can be understood from Lissajous plots.

Zero-strain nonlinearity (Q_o) of HSA-urea hydrogels

The zero-strain intrinsic nonlinear parameter (Q_o) (Hyun and Wilhelm 2009), can effectively characterize nonlinearities in several polymeric systems. In the FT-rheology framework, the Q parameter is given by $Q = I_{3/1}/\gamma_o^2$. The parameter Q_o is a strain independent value obtained when considering that Q tends to a constant value (Q_o) in the limiting case where $\gamma_o \to 0$. Therefore, Q_o provides a quantitative measure of nonlinearity. By fitting the function $[Q = Q_o\left(1 + \left(C_1\gamma_o\right)^{C_2}\right)^{(C_3-1)/C_2}]$ to the $Q(\gamma_o)$ plot (Kim and Hyun 2021), Q_o was obtained for the 7 wt.% HSA hydrogels containing 0–5 M urea (Fig. 6a). The $I_{3/1}$ and Q values of the 3 wt.%–7 wt.% HSA hydrogels with 0–5 M urea are shown in Fig. S9. The nonlinear behavior of the HSA-urea hydrogels, as quantified by Q_o, decreased quadratically with increasing urea concentrations (Fig. S10a). In their first studies, Hyun and Wilhelm (2009) found Q_o was sensitive to polymer topology, for example, Q_o values were lower for comb polystyrene with entangled branches compared to the unentangled counterparts.

Interestingly, for 5 wt.% and 7 wt.% HSA hydrogels containing 0–5 M urea, normalized G' linearly fits with their corresponding normalized Q_o values (Fig. S10b). This linear relationship is characterized by an average slope of 0.87, suggesting a direct correlation between nonlinearity and cross-linking density. The relative decline in the degree of intrinsic nonlinearity is attributed to urea displacing the hydrogel's hydrogen bond network (see Fig. 4b), which subsequently reduces the cross-linking density of HSA chains. This is further supported by the fact that G' in the SAOS regime is proportional to the hydrogel's cross-linking density. Hence, it is suggested that the source of the gel nonlinearity (Q_o) is the crosslinked HSA gel matrix.

Yielding behavior of HSA-urea hydrogels

Two commonly used critical strain amplitudes, along with the flow transition index (FTI) (Song et al. 2022b), were used to characterize the effect of HSA and urea concentrations on the yielding of HSA-urea hydrogels. Figure 6b shows the first critical yield strain (γ_y), second critical yield strain (γ_f), and the FTI of the 7 wt.% HSA hydrogels containing 0–5 M urea. The microscopic yielding is characterized by γ_y, which has been defined as the strain where the storage modulus decreases to 90% of its SAOS value, i.e., the strain amplitude where $G' = 0.9G_{SAOS}'$. For 7 wt.% HSA, the value of γ_y increased from 1 for the pure HSA hydrogel to a plateau value of 2.5 at 3 and 5 M urea. The macroscopic yielding

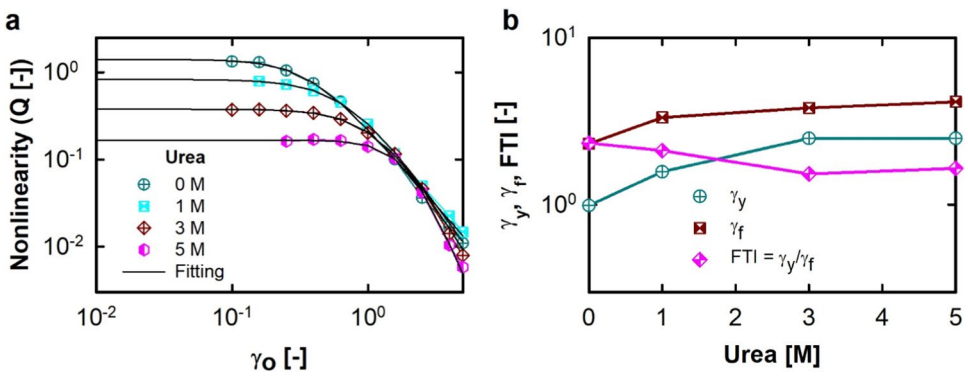

Fig. 6 (**a**) Variation of nonlinearity (Q) with strain amplitude; solid lines represent the fitting considering the function $Q = Q_o\left(1 + \left(C_1\gamma_o\right)^{C_2}\right)^{(C_3-1)/C_2}$. (**b**) First ($\gamma_y$) and second ($\gamma_f$) critical yield strain, and flow transition index (FTI) for the 7 wt.% HSA hydrogels containing 0–5 M of urea

is characterized by γ_f, which is observed when enough microscopic yielding has accumulated within the material's volume to cause viscous dissipation to predominate over the elastic behavior, i.e., the strain amplitude where $G' = G''$. The γ_f value increased with increasing urea, suggesting a delay in macroscopic fracturing of the gel matrix. The flow transition index, $FTI = \gamma_f/\gamma_y$ indicates the rapidity with which deformation changes from elastic dominance to flow dominance with increase in urea concentration. The FTI value of the pure 7 wt.% HSA hydrogel was 2.3, which decreased to approximately 1.6 for the hydrogels containing 3 and 5 M urea.

Roughly, the FTI and yielding properties of the gel matrix obtained from the critical strain amplitudes analysis exhibit a tradeoff relationship, as improved yielding also coincided with a rapid transition to flow-dominance post-yielding. The increase in protein-urea hydrogen bonding, and the accompanying decrease in HSA chain cross-linking density, are expected to lead to the observed increase in yield strain through improved stress dissipation.

SPP Analysis before and after yielding of HSA-urea hydrogels

The SPP moduli G_t' and G_t'' were calculated by differentiation following existing methods (Rogers et al. 2011; Rogers and Lettinga 2012; Rogers 2012; Choi et al. 2019; Erturk et al. 2022; Song et al. 2022a). It should be noted that G' and G'' in FT-rheology respectively represent the intracycle averaged elasticity and viscous dissipation and are calculated from the first stress harmonic (Mermet-Guyennet et al. 2015). However, the SPP moduli G_t' and G_t'' are transient values, not restricted to a particular harmonic, and may be obtained at any point during the cycle. The detailed transient deformational behavior of 7 wt.% HSA hydrogels containing 0–5 M urea are presented as Cole–Cole plots (G_t'' vs G_t') at $\gamma_o = 0.63$ (~ before yielding, Fig. 7) and at $\gamma_o = 1.58$ (~ after yielding, Fig. 8). The corresponding plots of 3 and 5 wt.% HSA hydrogels containing 0–5 M urea are presented at $\gamma_o = 0.63$ (Figs. S11–S12) and at $\gamma_o = 1.58$ (Figs. S13–S14). Additionally, elastic Lissajous curves are plotted for comparison against the Cole–Cole plots. The SPP Cole–Cole plots show that the HSA-urea hydrogel undergoes three different sequences of physical processes as follows: (i) structural breakdown to maximum during potential energy release, (ii) an early recovery, and (iii) structural recovery. The SPP Cole–Cole plots and Lissajous curves show that G_t' reaches a maximum (G_{tmax}') at [①] (i.e., at $\gamma(t) = \gamma_o$). Conversely, the peak of G_t'' (G_{tmax}'') was observed at [■] which corresponds to the region of strain amplitude from γ_o to 0. The increase in G_t'' until G_{tmax}'' likely occurs because the acquired potential energy is released as the structure returns toward the equilibrium position at② (i.e., at $\gamma(t) = 0$). The region [①→■] corresponds to the structural breakdown, which involves the loss of bonds such as hydrogen bonds, electrostatic contact, or crosslink points that lead to gradual yielding. In the region [■→●], G_t' remains unchanged or slightly increased; hence, the hydrogel is at an early recovery stage. However, beyond [●], G_t' increases in the positive direction as the hydrogel structure enters the recovery stage. Again, G_t' increases toward [①] until reaching a maximum at, or near, [①] where $\gamma(t) = \gamma_o$.

G_{tmax}' and G_{tmax}'' for the 7 wt.% HSA hydrogels containing 0–5 M urea obtained at $\gamma_o = 0.63$ and $\gamma_o = 1.58$ are presented in Tables 1 and 2, respectively. The signs + and – indicate an increase (+) or decrease (–) of the G_{tmax}' and G_{tmax}'' values between $\gamma_o = 0.63$ and $\gamma_o = 1.58$.

The G_{tmax}' and G_{tmax}'' of pure 7 wt.% HSA decreased by 67.08% and 68.16% respectively, at $\gamma_o = 1.58$ compared to the values at $\gamma_o = 0.63$. With 1 M urea, the corresponding decreases were 16.61% and 19.72%, respectively. However, at urea concentrations > 1M, an increase in G_{tmax}' and G_{tmax}'' was observed. The G_{tmax}' and G_{tmax}'' variations for the 3 wt.%–7 wt.% HSA hydrogels containing 0–5 M urea are shown in Fig. S15. At $\gamma_o = 0.63$, G_{tmax}' exhibited a behavior similar to that of G' from SAOS, i.e., it decreases with increasing urea concentration. However, at $\gamma_o = 1.58$, the G_{tmax}' value of urea-containing hydrogels were much higher than that of pure HSA hydrogels. The increase in the viscoelastic function with strain amplitude is common in biological gels and is referred to as strain hardening. The strain-hardening effect suggests that segments of the hydrogel network exhibit strain stiffening. The underlying origin is likely due to complex microstructures with segments resisting ongoing shear deformation (Hyun et al. 2011; Mermet-Guyennet et al. 2015). Thus, the behavior of G_{tmax}' and G_{tmax}'' confirms that the increase in urea produces microstructural changes and strain stiffening in the HSA hydrogels. In the deformation of several protein-containing flour doughs analyzed by SPP, the strain-hardening observed in the structural recovery process is attributed to the stretching of the gluten network, while the structural breakdown process is associated with the breakdown of the gluten network (Erturk et al. 2022).

Transient phase behavioral changes covering all strain amplitudes (SAOS to LAOS) of the hydrogels can be analyzed by the transient phase angle $\delta_t = \tan^{-1}(\frac{G_t''}{G_t'})$. A $\delta_t = \frac{\pi}{4}$ suggests equal viscous and elastic behavior, i.e., $G_t' = G_t''$; $\delta_t > \frac{\pi}{4}$ represents a greater viscous behavior; and $\delta_t < \frac{\pi}{4}$ represents a higher elastic behavior. For symmetry reasons, half of the oscillatory strain–stress cycle is sufficient (Fig. 9a). The colored portion of strain (green) and stress (red) are the only parts of the cycle that were considered. The color map of the transient phase angle behavior of the 7 wt.% HSA hydrogels containing 0–5 M urea are shown in Figs. 9b–e. The plots for 3 wt.%–5 wt.% with 0–5 M urea are presented

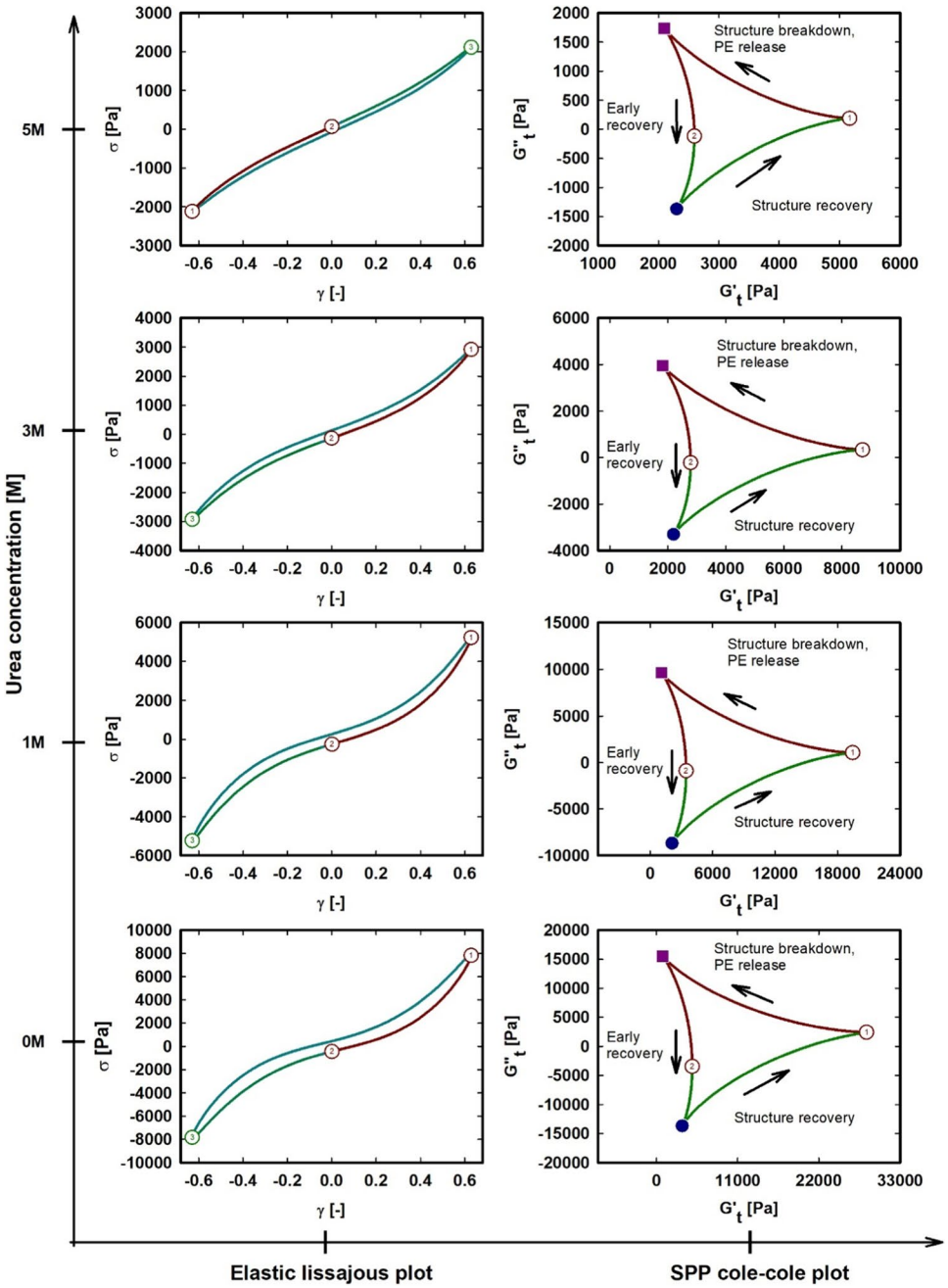

Fig. 7 Elastic Lissajous plots and SPP Cole–Cole plots of LAOS flow of 7wt.% HSA containing 0 – 5M urea at 1 rad/s and γ_o of 0.63

in Fig. S16. In all cases, the δ_t values ranged between −1.5 andl.5; however, the hydrogels' behavior is predominantly elastic (solid-like,$\delta_t < 0.79$), as expected.

All the hydrogels exhibited a uniform response until $\gamma_o = 0.16$ (SAOS region, Figs. 9b–9e) as observed by the uniformity in color. Beyond $\gamma_o = 0.16$, the appearance of bright yellow and dark blue, or stripes, indicate high viscous flows and strain-stiffening (strong elastic) responses, respectively. With the increase in urea concentration, the area of bright yellow and dark blue moved up on the map, to higher strain amplitude values. Hence, with increasing urea, the onset of nonlinear strain stiffening, and high viscous flows are delayed. The increase in hydrogel yield strains discussed above can be visualized here. In the nonlinear part of the color map, i.e., $\gamma_o > 0.16$), the hydrogels exhibit high viscous flows (bright yellow) and high strain stiffening (dark blue) in the segment $[\frac{\pi}{2} \rightarrow \frac{2\pi}{2}]$. Conversely, the flow behavior corresponds mainly to high strain stiffening in the segment $[\frac{2\pi}{2} \rightarrow \frac{3\pi}{2}]$. The first critical yielding is identified by the appearance of significant viscous flow (highlighted area, Figs. 9b–9e) in the $[\frac{2\pi}{2} \rightarrow \frac{3\pi}{2}]$ segment within the LAOS region. Thus, the color map allows for easy, yet comprehensive, qualitative identification of flow and yielding behavior, and to some extent, quantitative analysis. This approach is

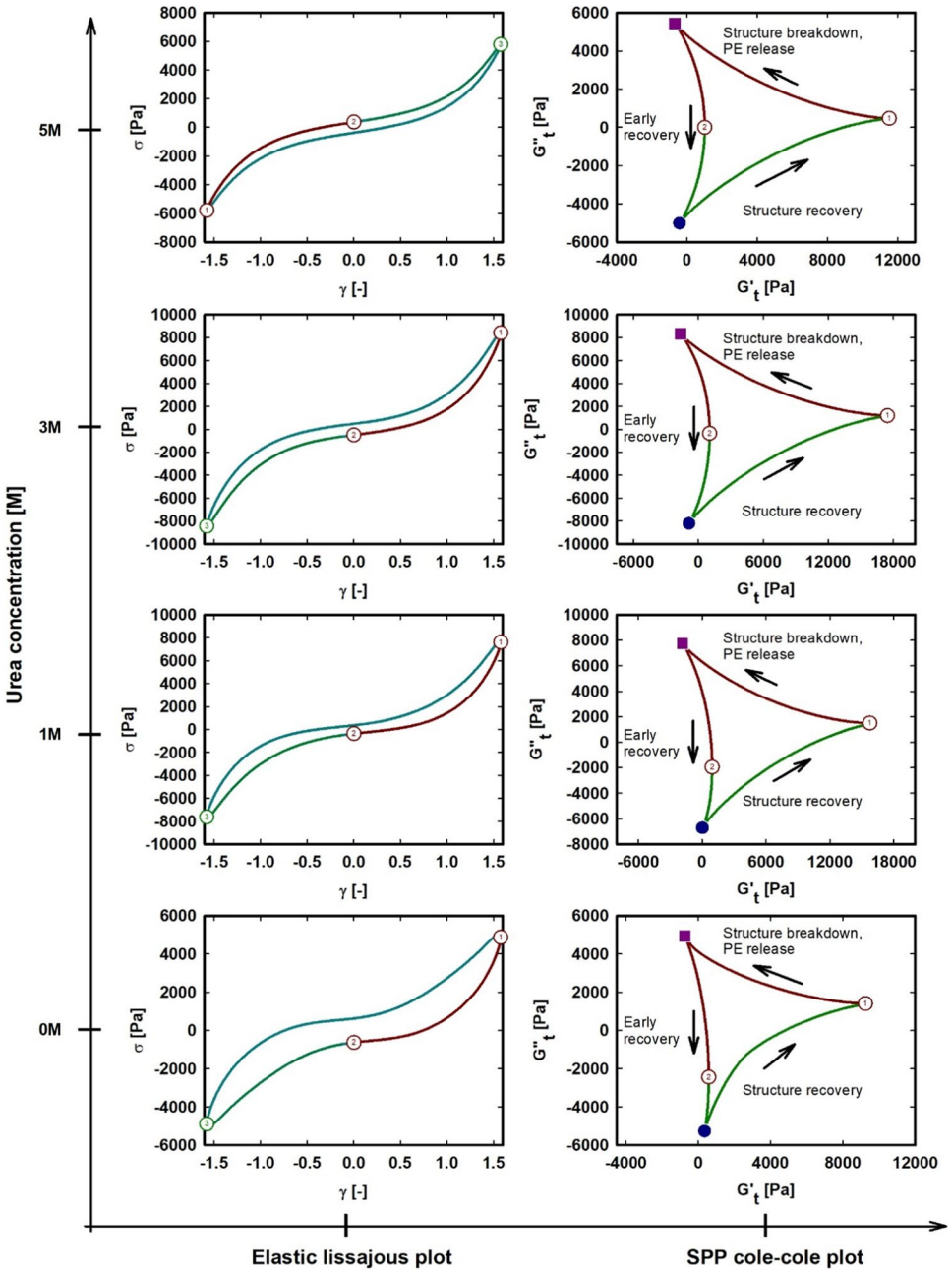

Fig. 8 Elastic Lissajous plots and SPP Cole–Cole plots of LAOS flow of 7 wt.% HSA containing 0 – 5M urea at 1 rad/s and γ_o of 1.58

Table 1 G_{tmax}' before ($\gamma_o = 0.63$) and after ($\gamma_o = 1.58$) yielding for the 7 wt.% HSA hydrogels containing 0 – 5 M urea

Urea [M]	G_{tmax}'[Pa]		Change
	[$\gamma_o = 0.63$]	[$\gamma_o = 1.58$]	
0	28992.47	9544.154	−67.080%
1	19548.42	16301.83	−16.610%
3	8711.772	17744.04	+103.68%
5	5177.5	11582.38	+123.71%

Table 2 G_{tmax}'' before ($\gamma_o = 0.63$) and after ($\gamma_o = 1.58$) yielding for the 7 wt.% HSA hydrogels containing 0 – 5 M urea

Urea [M]	G_{tmax}''[Pa]		Change
	[$\gamma_o = 0.63$]	[$\gamma_o = 1.58$]	
0	15523.92	4942.043	−68.160%
1	9648.004	7745.604	−19.720%
3	3950.295	8333.282	+110.95%
5	1734.379	5428.635	+213.00%

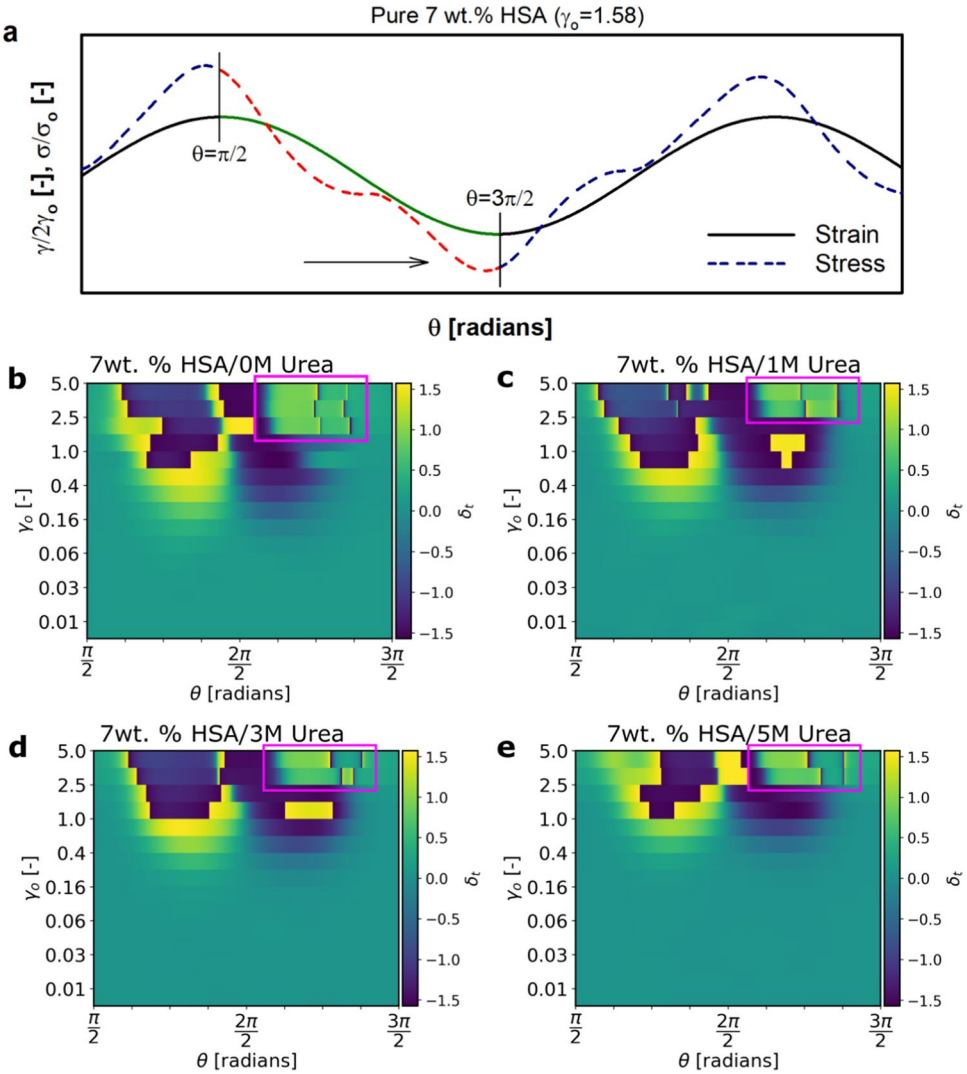

Fig. 9 (**a**) Oscillatory shear strain and stress for pure 7 wt.% HSA hydrogel at $\gamma_o = 1.58$ and (**b**)–(**e**) color map of the transient phase angle (δ_t) for the 7 wt.% HSA hydrogels containing 0–5 M urea. Transient properties are considered within a half cycle $[\frac{\pi}{2} \rightarrow \frac{3\pi}{2}]$. Colors indicate the dominant characteristic of the hydrogel at any point within the half cycle

expected to enable tailoring of the hydrogels' design, e.g., the choice of additives to achieve specific types of yielding, by analyzing the positions of yielding events in the deformation map.

Conclusions

The effect of urea on the linear and nonlinear rheological and microstructural responses of HSA and HSA-urea hydrogels was investigated through rheological characterization (temperature ramping, frequency sweep, and strain amplitude sweep tests), MD simulations, and observations from tube inversion tests.

During temperature ramping tests, solutions with pure HSA at 3 wt.%, 5 wt.%, and 7 wt.% were transformed into a hydrogel within a narrow T_{gel} range, exhibiting similar kinetics and viscoelastic properties proportional to protein concentration. However, T_{gel} decreased significantly as urea concentrations increased due to the rapid denaturation of HSA structures in the presence of urea.

Despite the rapid unfolding rate under increasing urea concentrations, the binding of urea to HSA through hydrogen bonding overall slowed the protein chains and subdued the driving forces of aggregation, resulting in a sparsely crosslinked 3D network structure. This can be inferred from SAOS tests, which show a decrease in viscoelastic properties and reduced frequency dependence of $G\prime$ and $G\prime\prime$. Nevertheless, all hydrogels, except 3 wt.% with more than 5 M urea, exhibited predominantly elastic behavior ($G\prime \gg G\prime\prime$) under the SAOS test in the range of 0.1–100 rad/s. All the hydrogels remained rigid when the tube inversion test was performed, except for the 3 wt.% HSA hydrogel containing more than 1 M urea, which exhibited viscous flow due to insufficient cross-linking.

To elucidate the atomic-level origin of the hydrogel behavior, MD simulations were carried out. This included secondary structure count and SASA results, which

confirmed that the HSA unfolding rate increased with urea concentration, leading to the rapid gelation of HSA in presence of urea. The urea RDF from the HSA surface, snapshots, and calculated diffusion coefficient confirmed the ease of urea integration into the HSA hydrogen bond network; however, the resultant complex suffered slowed protein dynamics leading to the observed changes in the HSA-urea hydrogel viscoelastic properties.

During the LAOS tests, both pure HSA and HSA-urea hydrogels showed nonlinear strain stiffening at large strain amplitudes. Hydrogel nonlinearity was quantified using the intrinsic nonlinear parameter Q_o. This increased with HSA but decreased with urea concentrations, suggesting that the nonlinear behavior is related to the cross-linking density of the gel matrix. The first and second critical yielding of the gel structure were delayed as urea concentration increased, indicating a tradeoff relationship with gel strength. The hydrogel under dynamic oscillatory shear was comprehensively visualized using a color map of the transient phase angle δ_t, defined using SPP parameters. The color map allowed for the localization of yielding events and offers further tailoring possibilities, such as the choice of additives to achieve novel yielding characteristics.

Supplementary Information The online version contains supplementary material available at https://doi.org/10.1007/s00397-024-01467-7.

Acknowledgements This research was supported by the National Research Foundation of Korea (NRF) grant funded by the Korean government (No. 2021R1I1A3054572).

Data availability The data that support the findings of this study are available from the corresponding author upon reasonable request.

Declarations

Conflict of interests The authors have no conflicts to disclose.

References

Arroyo V, García-Martinez R, Salvatella X (2014) Human serum albumin, systemic inflammation, and cirrhosis. J Hepatol 61:396–407. https://doi.org/10.1016/j.jhep.2014.04.01

Aufderhorst-Roberts A, Hughes MDG, Hare A, Head DA, Kapur N, Brockwell DJ, Dougan L (2020) Reaction rate governs the viscoelasticity and nanostructure of folded protein hydrogels. Biomacromol 21:4253–4260. https://doi.org/10.1021/acs.biomac.0c01044

Aufderhorst-Roberts A, Cussons S, Brockwell DJ, Dougan L (2023) Diversity of viscoelastic properties of an engineered muscle-inspired protein hydrogel. Soft Matter 19:3167–3178. https://doi.org/10.1039/d2sm01225a

Baler K, Martin OA, Carignano MA, Ameer GA, Vila JA, Szleifer I (2014) Electrostatic unfolding and interactions of albumin driven by ph changes: A molecular dynamics study. J Phys Chem B 118:921–930. https://doi.org/10.1021/jp409936v

Cao H, Duan Y, Lin Q, Yang Y, Gong Z, Zhong Y, Chen X, Shao Z (2019) Dual-loaded, long-term sustained drug releasing and thixotropic hydrogel for localized chemotherapy of cancer. Biomater Sci 7:2975–2985. https://doi.org/10.1039/c9bm00540d

Chen M-C, Ling M-H, Lai K-Y, Pramudityo E (2012) Chitosan microneedle patches for sustained transdermal delivery of macromolecules. Biomacromol 13:4022–4031. https://doi.org/10.1021/bm301293d

Choi J, Nettesheim F, Rogers SA (2019) The unification of disparate rheological measures in oscillatory shearing. Phys Fluids 31(7). https://doi.org/10.1063/1.5106378

Durham E, Dorr B, Woetzel N, Staritzbichler R, Meiler J (2009) Solvent accessible surface area approximations for rapid and accurate protein structure prediction. J Mol Model 15:1093–1108. https://doi.org/10.1007/s00894-009-0454-9

Erturk MY, Rogers SA, Kokini J (2022) Comparison of sequence of physical processes (SPP) and Fourier transform coupled with Chebyshev polynomials (FTC) methods to interpret large amplitude oscillatory shear (Laos) response of viscoelastic doughs and viscous pectin solution. Food Hydrocoll 128:107558. https://doi.org/10.1016/j.foodhyd.2022.107558

Fan Z-P, Li X-Y, Sun B, Sun C-L, Shi Z-F, Shao X-F, Zhang H-L (2022) Constructing two-dimensional crossed molecular packing through branching chain engineering of amino-indenofluorene derivatives. J Mater Chem C 10:8666–8673. https://doi.org/10.1039/d2tc01538b

French ME, Koehler CF, Hunter T (2021) Emerging functions of branched ubiquitin chains. Cell Discov 7:6. https://doi.org/10.1038/s41421-020-00237-y

Gasbarro NM, Solomon MJ (2019) Yield stress and rheology of a self-associating chitosan solution. Rheol Acta 58:729–739. https://doi.org/10.1007/s00397-019-01173-9

Ghosh A, Ali MA, Dias GJ (2009) Effect of cross-linking on microstructure and physical performance of casein protein. Biomacromol 10:1681–1688. https://doi.org/10.1021/bm801341x

Hájovská P, Chytil M, Kalina M (2020) Rheological study of albumin and hyaluronan-albumin hydrogels: effect of concentration, ionic strength, ph and molecular weight. Int J Biol Macromol 161:738–745. https://doi.org/10.1016/j.ijbiomac.2020.06.063

Hirose M, Tachibana A, Tanabe T (2010) Recombinant human serum albumin hydrogel as a novel drug delivery vehicle. Mater Sci Eng C 30:664–669. https://doi.org/10.1016/j.msec.2010.02.020

Hyun K, Wilhelm M (2009) Establishing a new mechanical nonlinear coefficient q from FT-rheology: first investigation of entangled linear and comb polymer model systems. Macromolecules 42:411–422. https://doi.org/10.1021/ma8017266

Hyun K, Kim SH, Ahn KH, Lee SJ (2002) Large amplitude oscillatory shear as a way to classify the complex fluids. J Non Newtonian Fluid Mech 107:51–65. https://doi.org/10.1016/s0377-0257(02)00141-6

Hyun K, Wilhelm M, Klein CO, Cho KS, Nam JG, Ahn KH, Lee SJ, Ewoldt RH, McKinley GH (2011) A review of nonlinear oscillatory shear tests: analysis and application of large amplitude oscillatory shear (Laos). Prog Polym Sci 36:1697–1753. https://doi.org/10.1016/j.progpolymsci.2011.02.002

Khodadadi S, Sokolov AP (2015) Protein dynamics: from rattling in a cage to structural relaxation. Soft Matter 11:4984–4998. https://doi.org/10.1039/c5sm00636h

Kim M, Hyun K (2021) Characterization of polyethylene/silica nanocomposites using different rheological analyses. Korea-Aust Rheol J 33:25–36. https://doi.org/10.1007/s13367-021-0003-3

Knox C, Law V, Jewison T, Liu P, Ly S, Frolkis A, Pon A, Banco K, Mak C, Neveu V, Djoumbou Y, Eisner R, Guo AC, Wishart DS (2011) DrugBank 3.0: A comprehensive resource for "OMICS" research on Drugs. Nucleic Acids Res 39:D1035–D1041. https://doi.org/10.1093/nar/gkq1126

Kong F, Mehwish N, Lee BH (2023) Emerging albumin hydrogels as personalized biomaterials. Acta Biomater 157:67–90. https://doi.org/10.1016/j.actbio.2022.11.058

Lawn RM, Adelman J, Bock SC, Franke AE, Houck CM, Najarian RC, Seeburg PH, Wion KL (1981) The sequence of human serum albumin cdna and its expression in E. coli. Nucleic Acids Res 9:6103–6114. https://doi.org/10.1093/nar/9.22.6103

Le Bon C, Nicolai T, Durand D (1999) Kinetics of aggregation and gelation of globular proteins after heat-induced denaturation. Macromolecules 32:6120–6127. https://doi.org/10.1021/ma9905775

Lee JS, Shin J, Park H-M, Kim Y-G, Kim B-G, Oh J-W, Cho S-W (2014) Liver extracellular matrix providing dual functions of two-dimensional substrate coating and three-dimensional injectable hydrogel platform for Liver Tissue Engineering. Biomacromol 15:206–218. https://doi.org/10.1021/bm4015039

Lemkul JA, Allen WJ, Bevan DR (2010) Practical considerations for building gromos-compatible small-molecule topologies. J Chem Inf Model 50:2221–2235. https://doi.org/10.1021/ci100335w

Li Q, Yu X, Zhang S, Xu M, Yang Y, Wan Z, Yang X (2023) All-natural, robust, and ph-responsive glycyrrhizic acid-based double network hydrogels for controlled nutrient release. ACS Appl Mater Interfaces 15:43633–43647. https://doi.org/10.1021/acsami.3c10407

Lu S, Yang Y, Yao J, Shao Z, Chen X (2016) Exploration of the nature of a unique natural polymer-based thermosensitive hydrogel. Soft Matter 12:492–499. https://doi.org/10.1039/c5sm01947h

Mermet-Guyennet MRB, Gianfelice de Castro J, Habibi M, Martzel N, Denn MM, Bonn D (2015) Laos: the strain softening/strain hardening paradox. J Rheol 59:21–32. https://doi.org/10.1122/1.4902000

Morris JF (2009) A review of microstructure in concentrated suspensions and its implications for rheology and bulk flow. Rheol Acta 48:909–923. https://doi.org/10.1007/s00397-009-0352-1

Nicolai T (2019) Gelation of food protein-protein mixtures. Adv Colloid Interface Sci 270:147–164. https://doi.org/10.1016/j.cis.2019.06.006

Nnyigide OS, Hyun K (2020) The protection of bovine serum albumin against thermal denaturation and gelation by sodium dodecyl sulfate studied by rheology and molecular dynamics simulation. Food Hydrocoll 103:105656. https://doi.org/10.1016/j.foodhyd.2020.105656

Nnyigide OS, Hyun K (2021) Molecular dynamics studies of the protective and destructive effects of sodium dodecyl sulfate in thermal denaturation of hen egg-white lysozyme and bovine serum albumin. J Biomol Struct Dyn 39:1106–1120. https://doi.org/10.1080/07391102.2020.1726209

Nnyigide OS, Hyun K (2023) A comprehensive review of food rheology: Analysis of experimental, computational, and Machine Learning Techniques. Korea-Aust Rheol J 35:279–306. https://doi.org/10.1007/s13367-023-00075-w

Nnyigide OS, Hyun K (2023) Charge-induced low-temperature gelation of mixed proteins and the effect of ph on the gelation: A spectroscopic, rheological and coarse-grained molecular dynamics study. Colloids Surf B Biointerfaces 230:113527. https://doi.org/10.1016/j.colsurfb.2023.113527

Nnyigide OS, Lee S-G, Hyun K (2018) Exploring the differences and similarities between urea and thermally driven denaturation of bovine serum albumin: intermolecular forces and solvation preferences. J Mol Model 24:75. https://doi.org/10.1007/s00894-018-3622-y

Nnyigide OS, Nnyigide TO, Hyun K (2021) The degradation of xanthan gum in Ionic and non-ionic denaturants studied by rheology and molecular dynamics simulation. Carbohydr Polym 251:117061. https://doi.org/10.1016/j.carbpol.2020.117061

Nnyigide OS, Nnyigide TO, Lee S-G, Hyun K (2022) Protein repair and analysis server: A web server to repair PDB structures, add missing heavy atoms and hydrogen atoms, and assign secondary structures by amide interactions. J Chem Inf Model 62:4232–4246. https://doi.org/10.1021/acs.jcim.2c00571

Nnyigide TO, Nnyigide OS, Hyun K (2023) Rheological and molecular dynamics simulation studies of the gelation of human serum albumin in anionic and cationic surfactants. Korean J Chem Eng 40:1871–1881. https://doi.org/10.1007/s11814-023-1513-0

Noteborn WEM, Gao Y, Jesse W, Kros A, Kieltyka RE (2017) Dual-crosslinked human serum albumin-polymer hydrogels for affinity-based drug delivery. Macromol Mater Eng 302(10):1700243. https://doi.org/10.1002/mame.201700243

Ollier RC, Xiang Y, Yacovelli AM, Webber MJ (2023) Biomimetic strain-stiffening in fully synthetic dynamic-covalent hydrogel networks. Chem Sci 14:4796–4805. https://doi.org/10.1039/d3sc00011g

Oostenbrink C, Villa A, Mark AE, Van Gunsteren WF (2004) A biomolecular force field based on the free enthalpy of hydration and solvation: the Gromos Force-field parameter sets 53A5 and 53A6. J Comp Chem 25:1656–1676. https://doi.org/10.1002/jcc.20090

Pieklarz K, Jenczyk J, Modrzejewska Z, Owczarz P, Jurga S (2022) An investigation of the sol-gel transition of chitosan lactate and chitosan chloride solutions via rheological and NMR studies. Gels 8:670. https://doi.org/10.3390/gels8100670

Piquero-Casals J, Morgado-Carrasco D, Granger C, Trullàs C, Jesús-Silva A, Krutmann J (2021) Urea in dermatology: a review of its emollient, moisturizing, keratolytic, skin barrier enhancing and antimicrobial properties. Dermatol Ther (heidelb) 11:1905–1915. https://doi.org/10.1007/s13555-021-00611-y

Rogers SA (2012) A sequence of physical processes determined and quantified in Laos: an instantaneous local 2D/3D approach. J Rheol 56:1129–1151. https://doi.org/10.1122/1.4726083

Rogers SA, Lettinga MP (2012) A sequence of physical processes determined and quantified in large-amplitude oscillatory shear (Laos): application to theoretical nonlinear models. J Rheol 56:1–25. https://doi.org/10.1122/1.3662962

Rogers SA, Erwin BM, Vlassopoulos D, Cloitre M (2011) A sequence of physical processes determined and quantified in Laos: application to a yield stress fluid. J Rheol 55:435–458. https://doi.org/10.1122/1.3544591

Song HY, Park SY, Kim S, Youn HJ, Hyun K (2022) Linear and nonlinear oscillatory rheology of chemically pretreated and non-pretreated cellulose nanofiber suspensions. Carbohydr Polym 275:118765. https://doi.org/10.1016/j.carbpol.2021.118765

Song HY, Park SY, Kim MC, Park JD, Youn HJ, Hyun K (2022a) A comparative study of the nonlinear rheological properties of three different cellulose nanofibril suspensions. Phys Fluids 34(5). https://doi.org/10.1063/5.0089656

Sugio S, Kashima A, Mochizuki S, Noda M, Kobayashi K (1999) Crystal structure of human serum albumin at 2.5 Å Resolution. Protein Eng 12:439–446. https://doi.org/10.1093/protein/12.6.439

Suman K, Shanbhag S, Joshi YM (2023) Large amplitude oscillatory shear study of a colloidal gel near the critical state. J Chem Phys 158:054907. https://doi.org/10.1063/5.0129416

Tarashi S, Nazockdast H, Bandegi A, Shafaghsorkh S, Sodeifian G, Foudazi R (2023) Large amplitude oscillatory shear behavior of thermoresponsive hydrogels: single versus double network. J Rheol 67:15–33. https://doi.org/10.1122/8.0000457

Turco G, Donati I, Grassi M, Marchioli G, Lapasin R, Paoletti S (2011) Mechanical spectroscopy and relaxometry on alginate hydrogels: A comparative analysis for structural characterization and network mesh size determination. Biomacromol 12:1272–1282. https://doi.org/10.1021/bm101556m

Wang C-S, Virgilio N, Carreau PJ, Heuzey M-C (2021) Understanding the effect of conformational rigidity on rheological behavior and formation of polysaccharide-based hybrid hydrogels. Biomacromol 22:4016–4026. https://doi.org/10.1021/acs.biomac.1c00803

Winter HH, Chambon F (1986) Analysis of linear viscoelasticity of a crosslinking polymer at the gel point. J Rheol 30:367–382. https://doi.org/10.1122/1.549853

Xia W, Siu WK, Sagis LMC (2021) Linear and non-linear rheology of heat-set soy protein gels: effects of selective proteolysis of β-conglycinin and glycinin. Food Hydrocoll 120:106962. https://doi.org/10.1016/j.foodhyd.2021.106962

Xiang X, Guo L, Wu X, Ma X, Xia Y (2012) Urea formation from carbon dioxide and ammonia at atmospheric pressure. Environ Chem Lett 10:295–300. https://doi.org/10.1007/s10311-012-0366-2

Yan C, Pochan DJ (2010) Rheological properties of peptide-based hydrogels for biomedical and other applications. Chem Soc Rev 39:3528–3540. https://doi.org/10.1039/b919449p

Yang YJ, Kim CS, Choi B-H, Cha HJ (2015) Mechanically durable and biologically favorable protein hydrogel based on elastic Silklike protein derived from sea anemone. Biomacromol 16:3819–3826. https://doi.org/10.1021/acs.biomac.5b01130

Zhang KY, Li D, Wang Y, Wang LJ (2023) Carboxymethyl chitosan/polyvinyl alcohol double network hydrogels prepared by freeze-thawing and calcium chloride cross-linking for efficient dye adsorption. Int J Biol Macromol 253:126897. https://doi.org/10.1016/j.ijbiomac.2023.126897